

# Evidence for nonlinear processes in fostering a North Pacific jet retraction

Melissa Breeden<sup>1</sup>  | Jonathan E. Martin<sup>2</sup>

<sup>1</sup>Atmospheric and Oceanic Sciences, Space Science and Engineering Center, University of Wisconsin-Madison, Madison, Wisconsin

<sup>2</sup>Department of Atmospheric and Oceanic Sciences, University of Wisconsin-Madison, Madison, Wisconsin

## Correspondence

Melissa Breeden, Space Science and Engineering Center, University of Wisconsin-Madison, 1225 W. Dayton St., Madison, WI 53706, USA.  
Email: mbreeden@wisc.edu

## Funding information

National Science Foundation, 1265182.

A diagnostic method for calculating local geostrophic wind tendencies in a piecewise manner within the quasi-geostrophic framework is introduced. The method is applied to a case-study of a North Pacific jet retraction that occurred in February 2006, and suggests that nonlinear interactions, which are dependent upon the phasing between potential vorticity anomalies and height anomalies, can lead to a weakening of the jet. The synoptic context in which nonlinear advection weakens the jet is presented, revealing that a positively tilted wave train situated north of the jet is conducive to retraction. This circumstance is consistent with conditions associated with barotropic energy extraction in which the growth of eddies occurs at the expense of the kinetic energy of the mean state. The relationship between this new method and existing methods of assessing geostrophic wind tendencies is explored and, though broad consistency is found, importance differences are identified and considered.

## KEYWORDS

jet stream variability, midlatitude weather systems, North Pacific atmospheric variability, vortex–vortex interactions

## 1 | INTRODUCTION

The zonal extension or retraction of the tropopause-level jet stream is intimately linked to the position and strength of a host of extratropical disturbances including cyclones, blocks and atmospheric rivers (Berggren *et al.*, 1949; Rex, 1950; Martius *et al.*, 2007; Jaffe *et al.*, 2011; Handlos and Martin, 2016; Griffin and Martin, 2017). In the North Pacific, the zonal pulsing of the jet exit region between 160°E and 160°W dominates tropopause-level zonal wind variability (Eichelberger and Hartmann, 2007; Athanasiadis *et al.*, 2010; Jaffe *et al.*, 2011; Griffin and Martin, 2017). The retracted phase of this pulsing North Pacific jet, wherein the jet exit region is nearer its western limit, is associated with more frequent subtropical cyclogenesis in the central part of the basin and midlatitude blocking in the north (Otkin and Martin, 2004; Breeden and Martin, 2018). The most notable impacts are on Hawaiian precipitation, but Jaffe *et al.* (2011) examined the composite evolution of 17 robust retractions from 1980 to 2007 and found that a persistent trough–ridge pattern developed over North America 5 days following retraction onset (their fig. 7), resembling the negative phase of the

Pacific–North American teleconnection pattern (Wallace and Gutzler, 1981). While periods of retraction and the attendant wavy (and often blocked) flow are well-known forecast challenges (Renwick and Wallace, 1996; Winters *et al.*, 2019), and are associated with notable sensible weather impacts such as flooding over Hawaii and the west coast of North America as well as extreme cold (Hoskins and Sardeshmukh, 1987; Otkin and Martin, 2004; Jayawardena *et al.*, 2012), a complete understanding of the transition to such a retracted state is lacking in the current literature. Various physical mechanisms for blocking onset and blocking maintenance have been attributed to deformation, vortex–vortex interactions, diabatic heating and tropical convection, but consensus regarding which of these processes is the most important has not yet been achieved (Frederiksen, 1983; Shutts, 1983; Yamazaki and Itoh, 2013; Pfahl *et al.*, 2015; Henderson *et al.*, 2016; Nakamura and Huang 2017). In this study we investigate the context in which quasi-geostrophic processes, representing purely dry dynamics, can contribute to a weakening of the typically strong North Pacific jet.

Shutts (1983) discussed how transient disturbances lead to the continued differential advection of low potential vorticity

(PV) into a midlatitude block, thereby reinforcing the block. Andrews and McIntyre (1976) first linked eddy momentum and temperature flux convergence, as represented by the Eliassen–Palm (E–P) flux convergence, to a weakening or strengthening of the zonal-mean zonal wind. Hoskins *et al.* (1983), Plumb (1985) and Trenberth (1986) all presented formulations that expanded the two-dimensional E–P flux diagnostics to three dimensions, often referred to as the **E**-vector, and demonstrated how this diagnostic can be used to study changes in the geostrophic wind. The key insight is that differential **E**-vector convergence is linked to flux convergence of the quasi-geostrophic potential vorticity (QGPV), the forcing for Lagrangian changes in low-frequency QGPV, and thus influences the gradient of QGPV upon which the geostrophic wind is dependent. In this study, we extend QG piecewise tendency diagnosis (PTD; Nielsen-Gammon and Lefèvre, 1996), traditionally used to investigate height tendencies associated with an amplifying synoptic wave, to investigate the various physical processes and their direct influence upon the Eulerian tendency of the geostrophic wind. In doing so we attain physical insights similar to those gained by the **E**-vector perspective but through an Eulerian perspective unconstrained by assumptions of a zonally symmetric basic state, which applies to either transient or stationary features. The way in which PTD can be utilized to combine information about eddy life cycles with their direct impact on the zonal wind is also considered.

Breeden and Martin (2018) examined a long-lived jet retraction that began in mid-February 2006 and was associated with persistent Hawaiian precipitation and flooding. The synoptic overview of the case showed that anticyclonic (LC1) wave breaking events in the 315–330 K isentropic layer facilitated retraction (Features A, B in Figure 1; their fig. 5). First, Feature A amplified in the central Pacific from 11 to 15 February (Figure 1a–c) and proceeded to overturn anticyclonically thereafter (Figure 1d). Feature B moved through the jet core in the 315–330 K layer from 13 to 16 February, becoming superposed with A by 19 February (Figure 1e). To investigate the initial weakening of the jet, the life cycle of A was diagnosed using the PTD methodology introduced by Nielsen-Gammon and Lefèvre (1996). PTD employs QGPV inversion to identify various physical processes that influence the life cycle of a growing synoptic disturbance using QG height tendencies. Application of PTD to Feature A revealed that large-scale deformation in the background state governed its amplification, and in concert with baroclinic amplification and nonmodal growth, Feature A was able to grow rapidly in magnitude and size in the central Pacific.

Evans and Black (2003) diagnosed the composite evolution of long-lived 500 hPa anticyclones in the Aleutian Low region and found the dominance of linear terms over nonlinear terms in contributing to development. Breeden and Martin (2018) also found that linear terms contributed most strongly to the growth of Feature A, although nonlinear terms

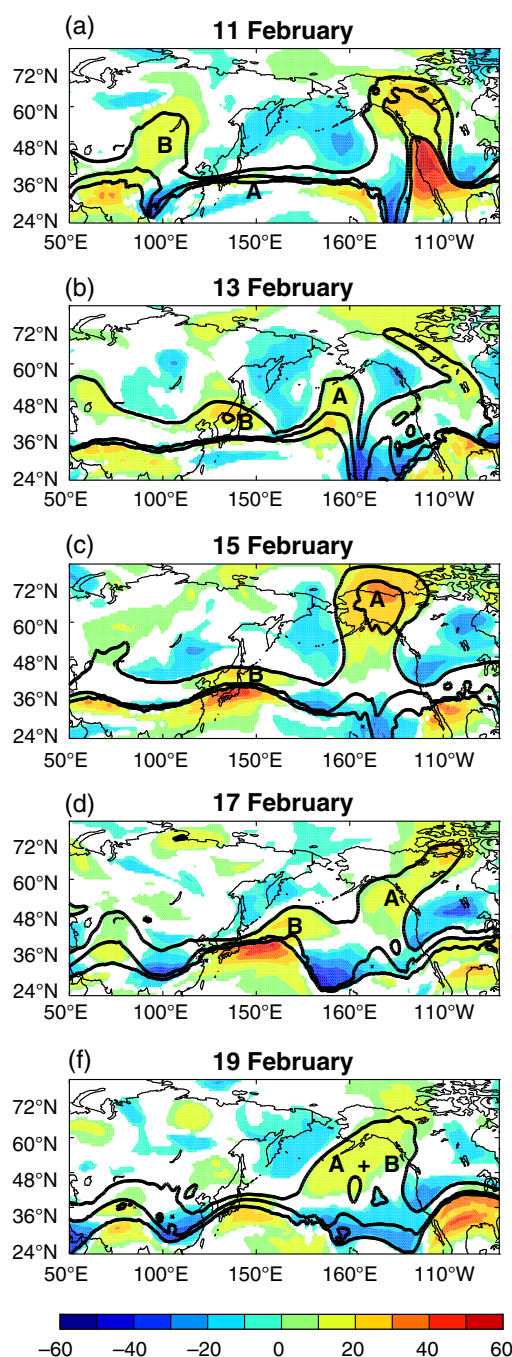


**FIGURE 1** Color shading shows the daily mean potential temperature anomalies on the 2PVU surface on (a) 11 (b) 13, (c) 15, (d) 17 and (e) 19 February 2006. Jet retraction criteria were met by 15–16 February (Jaffe *et al.*, 2011). The potential temperature anomalies were calculated with respect to the 1979–2015 climatology for each day. The contours show the total 315, 330 and 345 K potential temperature contours on the 2 PVU surface at each time. Anticyclonic anomalies A and B are labelled [Colour figure can be viewed at [wileyonlinelibrary.com](http://wileyonlinelibrary.com)].

did contribute to a lesser extent. In contrast to the North Pacific, Evans and Black (2003) found that North Atlantic persistent anticyclones amplified due to both nonlinear and linear processes. The results presented here, which emphasize how nonlinear processes can alter the North Pacific jet, have not been emphasized in previous studies that applied PTD to the North Pacific region.

In this article, the PTD methodology is expanded to quantify the explicit contributions from various physical processes, all distinguishable by PTD, to jet retraction: the deceleration of the jet in its exit region. The expanded PTD methodology is outlined in section 2 and is applied to the initial stage of the 2006 jet retraction in section 3. Discussion and conclusions comparing this diagnostic to other studies related to jet stream variability are presented in section 4.

## 2 | DATA AND METHODOLOGY

This study employs European Centre for Medium-range Weather Forecasting (ECMWF) ERA-Interim gridded data, accessed at  $1^\circ \times 1^\circ$  spatial resolution and six-hourly temporal resolution, via the online archive (Dee *et al.*, 2011). The ERA-Interim dataset optimally combines observations (including those from polar-orbiting and geostationary satellites) using a four-dimensional variational analysis (4D-Var) scheme, with model output, to create a reanalysis dataset from 1979 to the present. Geopotential was accessed on pressure surfaces from 50 to 1,000 hPa at 50 hPa intervals and was used for QGPV inversion, as well as height and geostrophic wind tendencies. Height anomalies at 300 hPa were calculated with respect to the 11–15 February 2006 average subtracted at each available time. Height tendencies at each grid point were computed using a 12 h, centred finite-difference approximation

$$\frac{\partial \phi}{\partial t} = \frac{\phi(t + \Delta t) - \phi(t - \Delta t)}{2\Delta t}, \quad (1)$$

where  $\Delta t = 6$  h. We will call these the “observed” height tendencies, which will be compared to those invertible from the QG system.

The dynamic tropopause was considered in terms of Ertel (1942) potential vorticity on the 2 PVU surface ( $1 \text{ PVU} = 10^{-6} \text{ K kg}^{-1} \text{ m}^2 \text{ s}^{-1}$ ). Potential temperature ( $\theta$ ) on the 2 PVU surface is provided by ECMWF and is determined by identifying the first observation of the 2 PVU value below 98 hPa, and then evaluating  $\theta$  at that grid point (Berrisford *et al.*, 2011). If the 2 PVU value is not located below 98 hPa, no value of  $\theta$  is included in the dataset. Potential temperature anomalies from the long-term mean were computed with respect to the 1979–2016 average at each available time, and then were averaged to a daily mean.

### 2.1 | Extended piecewise tendency diagnosis

The traditional PTD methodology was explained and applied in detail in Nielsen-Gammon and Lefèvre (1996) and Breeden and Martin (2018). If one assumes that quasi-geostrophic potential vorticity (QGPV, given in Equation 2) is conserved following geostrophic motion, QG height tendencies are directly related to geostrophic QGPV advection (Equation 3):

$$q = f + \frac{1}{f_0} \nabla^2 \phi + f_0 \frac{\partial}{\partial p} \left( \frac{1}{\sigma} \frac{\partial \phi}{\partial p} \right) = f + \mathcal{L}(\phi), \quad (2)$$

$$\frac{\partial \phi}{\partial t} = \mathcal{L}^{-1} \left( \frac{\partial q}{\partial t} \right) = \mathcal{L}^{-1}(-\mathbf{v}_g \cdot \nabla q). \quad (3)$$

Inverting advection will yield the corresponding QG height tendencies. By defining a basic state (overbars) and perturbations around that basic state (primes) and splitting the atmosphere into an upper and lower layer (denoted by subscripts “u” and “l”, respectively), advection can be split into several components that represent distinct physical processes. In this study the upper layer is defined from 500 to 50 hPa, and the lower layer from 1,000 to 550 hPa, corresponding to the QGPV, height and geostrophic wind fields  $q'_u$ ,  $\phi'_u$ ,  $\mathbf{v}'_{gu}$  and  $q'_l$ ,  $\phi'_l$ ,  $\mathbf{v}'_{gl}$ , respectively. Equation 4 below includes only the terms that contribute to  $\phi'_u$  tendencies, which represent the majority of the 300 hPa  $\phi'$  evolution. A full diagnosis of the evolution of  $\phi'$  would require investigation of advection of lower-level QGPV in addition to advection of the upper-level QGPV, adding six more terms to investigate to explain a much smaller fraction of the 300 hPa evolution:

$$\begin{aligned} \frac{\partial \phi'_u}{\partial t} = & \overset{i}{\mathcal{L}^{-1}(-\bar{\mathbf{v}}_g \cdot \nabla q'_u)} + \overset{ii}{\mathcal{L}^{-1}(-\mathbf{v}'_{gu} \cdot \nabla \bar{q}_u)} + \overset{iii}{\mathcal{L}^{-1}(-\mathbf{v}'_{gl} \cdot \nabla \bar{q}_u)} \\ & + \overset{iv}{\mathcal{L}^{-1}(-\mathbf{v}'_{gu} \cdot \nabla q_u)} + \overset{v}{\mathcal{L}^{-1}(-\mathbf{v}'_{gl} \cdot \nabla q_u)} + \overset{vi}{\mathcal{L}^{-1}(-\bar{\mathbf{v}}_g \cdot \nabla \bar{q}_u)}. \end{aligned} \quad (4)$$

The terms in Equation 4 include effects of tropopause-level deformation (Term *i*), downstream development (Term *ii*), baroclinic amplification (Term *iii*), perturbation nonlinear vortex–vortex interactions (Terms *iv*–*v*) and basic state nonlinear interactions (Term *vi*). Tracking the height tendencies at the centre of a growing wave provides a way to diagnose which processes contribute to intensification over the wave’s life cycle. If positive height tendencies from a given term overlap with a geopotential height maximum, for instance, that term promotes development, while negative height tendencies would indicate that term acts to weaken the height maximum. The sum of all terms indicates whether the anomaly strengthens or decays overall. For a more in-depth explanation of each term, the reader is referred to Nielsen-Gammon and Lefèvre (1996) or Breeden and Martin (2018).

### 2.2 | Geostrophic wind tendency equations

While understanding the life cycle of synoptic features that facilitate retraction is illuminating, the amplification of a given ridge or trough alone does not directly correspond to a specific impact on the zonal wind. Rather, the movement of eddies, as represented by their associated height tendencies, leads to changes in geostrophic wind speed. Taking the local time derivative of the geostrophic wind and rearranging the partial derivatives yields a relationship between the local time tendency of the geostrophic wind and the

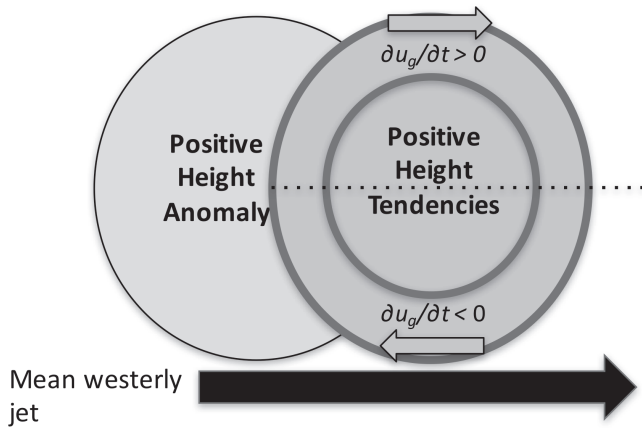


**FIGURE 2** Schematic demonstrating the distribution of the local change in the geostrophic zonal wind around a positive height tendency anomaly (see Equation (5a)). Where height tendencies increase with latitude, the zonal wind will weaken, and where height tendencies decrease with latitude, the zonal wind will strengthen (gray arrows). If the mean westerly jet is located south of the ridge, the height tendencies associated with the ridge will weaken the jet

horizontal gradient of local height tendencies:

$$\frac{\partial u_g}{\partial t} = -\frac{1}{f} \frac{\partial}{\partial y} \left( \left( \frac{\partial \phi}{\partial t} \right) \right) = -\frac{1}{f} \frac{\partial}{\partial y} \left( \mathcal{L}^{-1} \left( \frac{\partial q}{\partial t} \right) \right), \quad (5a)$$

$$\frac{\partial v_g}{\partial t} = \frac{1}{f} \frac{\partial}{\partial x} \left( \left( \frac{\partial \phi}{\partial t} \right) \right) = \frac{1}{f} \frac{\partial}{\partial x} \left( \mathcal{L}^{-1} \left( \frac{\partial q}{\partial t} \right) \right). \quad (5b)$$

Equation 5 reveals that if, in a certain location, the meridional gradient of height tendencies is positive, then the right-hand side of Equation 5a is negative, and the zonal geostrophic wind will weaken at that location (Figure 2). If, as in the schematic and the 2006 retraction, a short-wave, eastward-propagating ridge is located poleward of the mean jet axis, the ridge's movement will weaken the mean westerly flow. A similar tendency to weaken the zonal wind occurs on the northern branch of a trough, so a trough located *south* of the jet axis would similarly decelerate the jet. The aforementioned impact of troughs and ridges on the flow is far from a novel revelation, but when waves are periodic the influence on the geostrophic wind is often short-lived. By definition, jet retractions require that the zonal wind is weakened substantially (at least 10 m/s below climatology in the vicinity of the jet exit region (Jaffe *et al.*, 2011)) and for at least 5 days. Consequently, an impact beyond the transient, periodic movement of waves along the jet must be achieved by the eddies to explain the time-integrated transition of the jet. Determining which of the terms isolated in PTD accounts for this transition is the primary focus of this analysis.

Assuming QGPV is conserved following the geostrophic flow, geostrophic QGPV advection can be substituted for  $\frac{\partial q}{\partial t}$  in Equation 5a, and the same partitioning of advection as done in traditional PTD can be applied:

$$\frac{\partial u_g}{\partial t} = -\frac{1}{f} \frac{\partial}{\partial y} \left\{ \begin{array}{l} \mathcal{L}^{-1}(-\bar{v}_g \cdot \nabla q'_u) + \mathcal{L}^{-1}(-v'_{gu} \cdot \nabla \bar{q}_u) \\ + \mathcal{L}^{-1}(-v'_{gl} \cdot \nabla \bar{q}_u) + \mathcal{L}^{-1}(-v'_{gu} \cdot \nabla q'_u) \\ + \mathcal{L}^{-1}(-v'_{gl} \cdot \nabla q'_u) + \mathcal{L}^{-1}(-\bar{v}_g \cdot \nabla \bar{q}_u) \end{array} \right\}. \quad (6)$$

Equation 6 demonstrates that the local weakening and strengthening of the geostrophic wind can be diagnosed in a piecewise manner, similar to that by which height tendencies were diagnosed in traditional PTD. Here the zonal wind component alone is emphasized, as retractions are defined based upon zonal wind variability, which dominates jet variability in the North Pacific (Athanasiadis *et al.*, 2010; Griffin and Martin, 2017). One may track the changes to the zonal wind following a certain anomaly, such as Feature A, in a manner similar to that in which the maximum height anomaly associated with Feature A was tracked and diagnosed. Alternatively, it is possible to choose one location – for example, the jet exit region – and explore the processes accelerating the zonal wind in that region through time. Consistent with the Eulerian definition of jet retractions presented by Jaffe *et al.* (2011), the latter approach is used to understand how retraction was initiated in February 2006. Recall that the jet exit region in the central Pacific coincides with the location of greatest amplitude in the empirical orthogonal function (EOF1) pattern of the 300–250 hPa zonal wind (fig. 4 from Jaffe *et al.*, 2011). The next section investigates the cumulative influence of Features A and B on retraction from 11 to 15 February, using the same PTD results presented in Breeden and Martin (2018).

### 3 | RESULTS FROM APPLYING PIECEWISE ZONAL WIND TENDENCY DIAGNOSIS

Figure 3 shows the net zonal geostrophic wind change from 0000–1800 UTC 11 to 15 February, attained by summing the instantaneous zonal wind tendency calculated using the observed height tendency (Equation 1), for each 6-hourly time step in the five-day period. Over this 5-day period the zonal wind weakened substantially along the southern portion of the jet core as well as in its exit region near 160°W. Understanding what features and, through Equation 6 what processes, contributed to the retraction/deceleration of the zonal jet is the focus of the ensuing analysis. Retractions are focused on weakened zonal flow specifically within the climatological jet exit region in the central North Pacific, often associated with a split jet and a dipole-type block (Jaffe *et al.*, 2011). Figure 4 shows the time series of the deceleration calculated in a variety of ways, averaged over an area encompassing the jet exit region (green box in Figure 3). To ensure the deceleration captured by the anomalous upper-level height field accurately represents the change in the unpartitioned height field, the upper-level height anomaly field was attained by inverting the 50–500 hPa perturbation QGPV,  $q'_u$  (Equation 7). Subsequently, the local deceleration using the  $\phi'_u$  field was calculated via Equation 1:

$$\phi'_u = \mathcal{L}^{-1}(q'_u). \quad (7)$$

The close match between the two time series in Figure 4a confirms that the application of PTD via Equation 6 to diagnose the processes involved in retraction can be

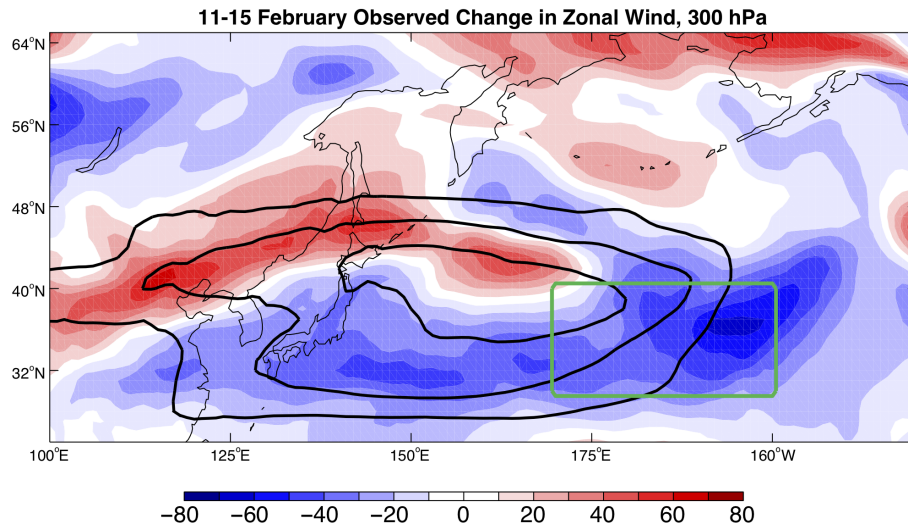


**FIGURE 3** Color shading shows the 11–15 February 2006 change in 300 hPa zonal wind in m/s. The contours show the 11–15 February mean geostrophic zonal wind, contoured starting at 30 m/s every 10 m/s. The green box indicates the region over which the retraction is diagnosed [Colour figure can be viewed at [wileyonlinelibrary.com](http://wileyonlinelibrary.com)].

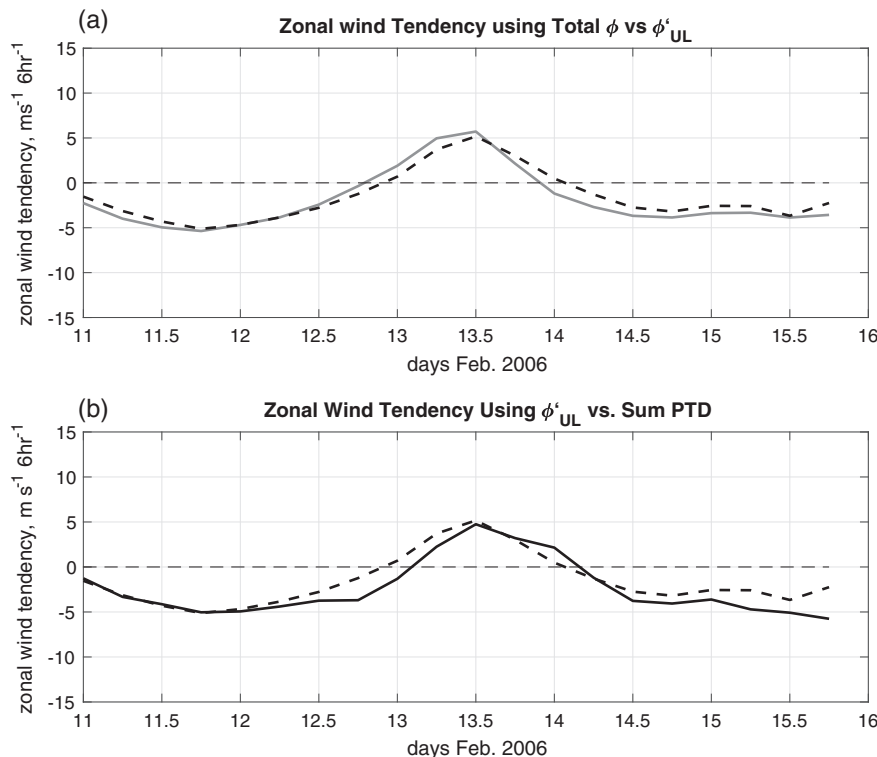


**FIGURE 4** Time series tracking 300 hPa zonal wind change (units  $\text{m s}^{-1} (6 \text{ h})^{-1}$ ) averaged from 30 to 40°N, 170 to 200°W, from 11 to 15 February, using six-hourly data. (a) Zonal wind tendency using the total height field (gray line) and the inverted height anomaly field associated with 50–500 hPa perturbation QGPV (black dashed line). (b) The black dashed line is as in (a), and the black solid line shows the zonal wind tendency explained using the height tendencies from PTD (Equation 6)

used to insightfully diagnose the observed changes in the tropopause-level jet. Both fields indicate that the zonal wind in the jet exit region weakened from 11 to 12 February, temporarily strengthened on 13 February, and then weakened from 14 to 15 February.

To quantify the net change in the zonal wind associated with the upper-level QGPV structure, the area under the blue line in Figure 4b was integrated, corresponding to an overall wind speed change of  $-32 \text{ m/s}$  from 0000–1800 UTC

11 to 15 February. The cumulative deceleration attained using the QG height tendencies output by PTD using Equation 6 implies a deceleration of 47 m/s. The discrepancy between the observed and PTD-induced wind speed change may derive from the assumptions within the QG system, including using the geostrophic wind in the advection terms and assuming adiabatic motion. The difference in the observed and PTD-attributed deceleration suggests that ageostrophic and diabatic processes may systematically oppose the strong

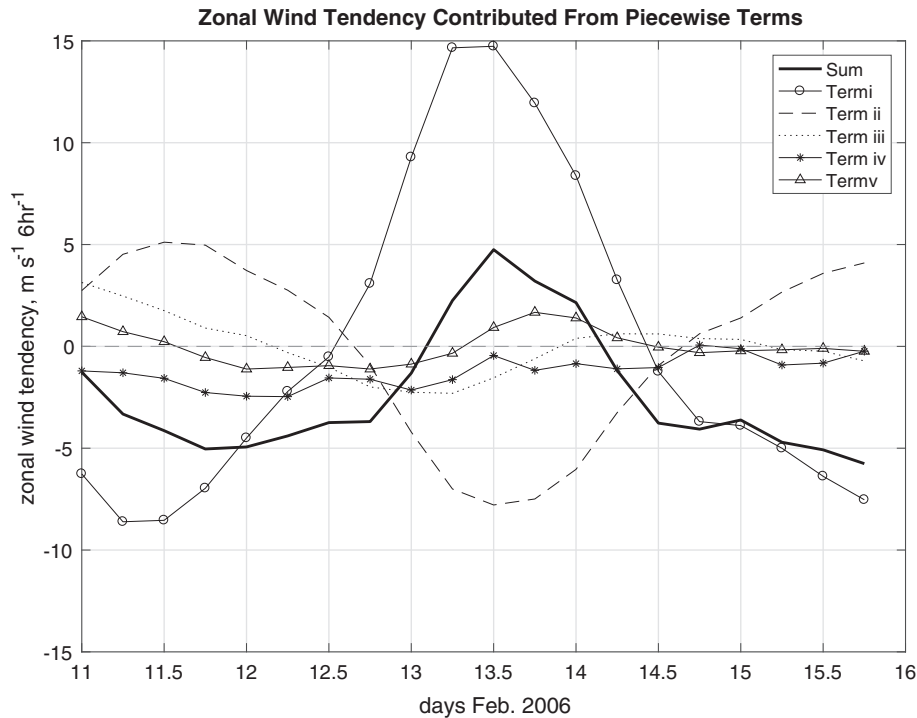


**FIGURE 5** Time series of the individual PTD components' contribution to the 300 hPa zonal wind tendency using Equation (6), from 0000 UTC 11 February to 1800 UTC 15 February. The black thick line is the sum of all terms, the black line with circles is Term *i*, black dashed line Term *ii*, black dotted line Term *iii*, black line with stars is Term *iv*, and black line with triangles is Term *v*

quasi-geostrophic forcing for height and geostrophic wind speed changes. Evans and Black (2003) expanded PTD to include these nonconservative effects, and while their inclusion did result in a better match with the observed evolution, they concluded that these processes were of secondary importance for understanding the dynamics of amplifying disturbances. While it is not our intent to perfectly recreate observations by employing the QG system, but rather to better understand the respective roles of the relevant dynamical processes involved in retraction, we maintain that investigation of the piecewise terms provides meaningful insight into the context and processes that can weaken the North Pacific jet, as will be demonstrated in the next section.

### 3.1 | Piecewise zonal wind tendency results

The terms that drove the amplification of Feature A (Terms *i* and *iii*: Breeden and Martin, 2018) are not necessarily the same terms that contributed most to the jet retraction. Figure 5 shows the time series of the deceleration arising from the terms in Equation 6, revealing that the highest-magnitude term is Term *i*, the propagation/deformation term ( $-\bar{v}_g \cdot \nabla q'_u$ ), which oscillates in concert with the total deceleration. This term includes the advection of ridges and troughs by the time mean geostrophic wind, so a large contribution from this term is not surprising. For example, Feature A propagated north of the boxed region from 11 to 12 February, when Term *i* produced a negative zonal wind tendency that was associated with the southern edge of the positive height tendencies associated with Feature A. Term *ii*, the downstream

development term ( $-\mathbf{v}'_{gu} \cdot \nabla \bar{q}_u$ ), represents the advection of the background QGPV gradient by the circulation associated with QGPV anomalies and varies inversely with the advection/deformation term and the total deceleration. As an example, consider how the northerly flow on the western side of a trough will lead to positive background QGPV advection and height falls, reflecting the trough's tendency to propagate upstream relative to the background wind. This upstream propagation is opposed by the background wind's tendency to advect the trough downstream, producing height *rises* west of the trough. As a result, the advection/deformation and downstream development terms are anticorrelated.

Term *iii*, the baroclinic development term ( $-\mathbf{v}'_{gl} \cdot \nabla \bar{q}_u$ ), first negated retraction on 11 February and then promoted it from 12 to 13 February. Thereafter this process made barely any direct contribution to the zonal geostrophic wind tendency. Interestingly, Term *iv*, upper-level, nonlinear vortex–vortex interactions ( $-\mathbf{v}'_{gu} \cdot \nabla q'_u$ ), which had a weaker influence on the amplification of Feature A than the previous terms, systematically contributed to retraction throughout the 5 days. The contribution to retraction from Term *v*, low-level nonlinear interactions, oscillated closely around zero. Finally, the large-scale nonlinear interaction term ( $-\bar{v}_g \cdot \nabla \bar{q}_u$ ), which is computed as an average deceleration over the five-day period, contributed to retraction as well (Table 1).

It was previously noted that the instantaneous change in zonal wind is heavily influenced by the transient movement of eddies into and out of the region where retractions are identified. The deformation and downstream development terms clearly demonstrate this oscillatory behaviour. The net

**TABLE 1** Integrated tendency of the 300 hPa zonal wind from 0000 UTC 11 February – 1800 UTC 15 February 2006 using various height tendency fields.

Height Field	Integrated Zonal Wind Tendency ( $\text{m s}^{-1}$ )
$q'_u$ - Derived Height Anomaly, $\phi'_u$	-31.8388
Unpartitioned zonal wind tend	-38.6878
<b>Total PTD</b>	<b>-47.6753</b>
Term <i>i</i> : Deformation/Superposition	-0.0079
Term <i>ii</i> : Downstream Development	-0.0186
Term <i>iii</i> : Baroclinic Development	-0.0100
Term <i>iv</i> : Vortex-vortex UL	-24.8444
Term <i>v</i> : Vortex-vortex LL	-0.2193
Term <i>vi</i> : Large-scale nonlinear term	-22.5752

changes in zonal wind from each term in Equation 6 were determined by summing each term's zonal wind tendency at each 6-hour time step over the 5-day period. The results shown in Table 1 reveal that the integrated effects of all terms *except* upper-level nonlinear interactions are near zero. Of course, the integrated contributions for the deformation, downstream development and baroclinic development terms *must* be near zero, since the integration was performed over the same period in which the anomalies were defined. It is thus possible some of the discrepancy between the PTD and observed deceleration is due to the fact that one of the linear terms negates retraction, which is not observed because all linear terms sum to zero over the 5-day period. The only terms that are not constrained to be zero in the integration are the nonlinear, vortex–vortex interaction terms, Terms *iv*, *v* and *vi*. Interestingly, in this case it is found that the two upper-level nonlinear interactions terms, *iv* and *vi*, accounted for the PTD-implied deceleration in the vicinity of the jet exit region. The context in which this was achieved is described in the next subsection.

Figure 6 shows the spatial maps of the average deceleration of the nonlinear terms from 11 to 15 February (the deformation, downstream development and baroclinic development components are near zero everywhere in the domain and thus are not shown). The two vortex–vortex interaction terms exhibit strong, often opposing dipoles of acceleration and deceleration that straddle the jet meridionally (Figure 6b,c). Local deceleration associated with upper-level vortex–vortex interactions was located within the jet exit region and southern portion of the jet core, accounting for half of the retraction diagnosed by the QG system. In the jet exit region, the basic state nonlinear interaction term also produced a meridionally oriented dipole pattern, inducing a negative zonal wind tendency to the south and within the box used to track retraction, and a positive zonal wind tendency to the north. The influence of Term *iv* is consistent with the perspective of Hoskins *et al.* (1983) and Shutts (1983), who both emphasized nonlinear potential vorticity flux convergence as forcing that weakens the *Lagrangian* tendency of the QGPV. If the QGPV tendencies are non-uniform, the QGPV

gradient will also change, corresponding to changes in the zonal wind.

### 3.2 | Investigation of upper-level vortex–vortex interactions

To contextualize the conditions during which upper-level vortex–vortex interactions produced retraction, Figure 7a shows the 12 February mean forcing for Term *iv*, with the associated positive height tendency response shown in Figure 7b. The fill in Figure 7a shows the  $q'_u$  anomalies that are advected by  $\mathbf{v}'_{gu}$ , shown by the arrows. Recall that  $\mathbf{v}'_{gu}$  is computed from  $\phi'_u$ , which in turn is related to the same  $q'_u$  field that is being advected. Due to the slight offset between  $\phi'_u$  and  $q'_u$  (resulting from the non-local influence of each QGPV anomaly in the domain) the geostrophic circulation  $\mathbf{v}'_{gu}$  is not perfectly parallel to isopleths of  $q'_u$  and thus advection is possible.

Regions of negative QGPV advection produce positive height tendencies (Equation 3), which are, in turn, associated with deceleration on their southern edge (Figure 2; Equation 5a). Negative QGPV advection is particularly notable on the eastern portion of Feature A, at this time located at 45°N, 175°W, with strong northerly winds producing negative advection of  $q'_u$  to the south. In fact, both Features A and B are associated with strong, negative  $q'_u$  anomalies that were greatest in magnitude near 45°N, and northerly flow on each anomaly's eastern side advected low  $q'_u$  southward. Simultaneously, southerly flow on the western side of A and the eastern flank of the trough upstream advected subtropical negative  $q'_u$  northward, forcing height rises centred at 35°N, 150°E. The coordinated negative  $q'_u$  advection associated with A, B and the trough in between produced a nearly continuous region of height rises extending from 110°E to 160°W (Figure 7b). To the south of this strip of height rises, a negative zonal geostrophic wind tendency was produced (Figure 7c, blue contours). The location of the negative zonal wind tendency with respect to the zonal jet on 12 February confirms that both the exit region and southern edge of the jet core were induced to weaken by this term.

### 3.3 | Investigation of large-scale nonlinear interactions

In conjunction with the previous term, large-scale nonlinear interactions also aided in the deceleration of the jet exit region. This term leads to height changes when the environmental geostrophic wind,  $\bar{\mathbf{v}}_g$ , crosses the background QGPV gradient,  $\nabla \bar{q}_u$ . At 300 hPa, while  $\bar{\mathbf{v}}_g$  is mostly parallel to the 300 hPa background QGPV gradient, it is possible that the influence of the lower-level QGPV gradient can influence  $\bar{\mathbf{v}}_g$  and induce advection, as is observed from 11 to 15 February (Figure 8). Near the date-line from 35 to 40°N, the 850 hPa  $\bar{\phi}$  is characterized by a broad trough, and southwesterly flow on its southeastern side crosses the 300 hPa background QGPV gradient (Figure 8a), leading to negative

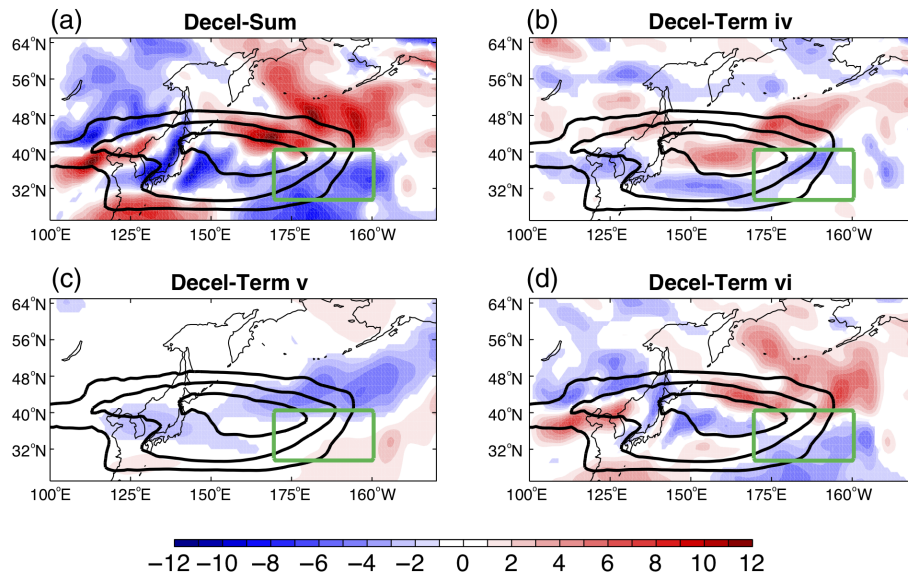


**FIGURE 6** Color shading shows the 300 hPa averaged zonal wind tendency from 0000 UTC 11 February to 1800 UTC 15 February 2006 from terms in Equation (6) in m/s. (a) Sum of Terms  $i-v_i$ , (b) Term  $iv$  ( $-\mathbf{v}'_{gu} \cdot \nabla q'_u$ , upper-level vortex–vortex interactions), (c) Term  $v$  ( $-\mathbf{v}'_{gl} \cdot \nabla q'_u$ , low-level vortex–vortex interactions) and (d) Term  $vi$  ( $-\mathbf{v}'_g \cdot \nabla q'_u$ , large-scale nonlinear interactions). Average wind speed tendencies less than a magnitude of 1 m/s ( $6 \text{ h}^{-1}$ ) are whited out. The contours in each plot are the same and show the 11–15 February mean geostrophic wind, contoured starting at 30 m/s at intervals of 10 m/s. The green box showing the region used to track the retraction of the jet exit region is shown in each figure [Colour figure can be viewed at [wileyonlinelibrary.com](http://wileyonlinelibrary.com)].

QGPV advection and height rises (Figure 8b). On the southern edge of the height rises, a negative zonal geostrophic wind tendency is produced, which is located on the southeastern portion of the jet (Figure 8b). Conversely, northwesterly flow on the large-scale 850 hPa trough's western edge produces positive QGPV advection and height falls. On the northern edge of these height falls, the tendency of the zonal geostrophic wind is also negative, producing the observed pattern in Figure 8b and a tendency to weaken the zonal wind on the northern portion of the jet entrance region. The impact of the large-scale nonlinear term on the geostrophic wind is thus spatially different compared to the influence of the smaller-scale eddies captured in Term  $iv$ . However, both terms conspire to weaken the zonal wind in the vicinity of the jet exit region, despite the differences in the pattern of the induced height and zonal wind tendencies over the broader North Pacific region.

#### 4 | DISCUSSION AND CONCLUSIONS

In this article a novel perspective for understanding geostrophic wind speed changes through extension of the PTD diagnostics introduced by Nielsen-Gammon and Lefèvre (1996) was presented. It was shown that the simple relationship between horizontal gradients in height tendencies and changes in the geostrophic wind holds for instantaneous or time-averaged changes in the geostrophic wind. This relationship can be combined with piecewise tendency analysis to split the total deceleration field into contributions from various distinct processes, to eliminate the transient effect of wave propagation without requiring time or zonal averaging. The extended approach was applied to investigate the onset

of a long-lived North Pacific jet retraction in mid-February 2006. Specifically, the influence of a wave train containing positively-tilted, potent anticyclonic anomalies A and B north of the jet axis on the local deceleration that initiated retraction was quantified. The impact of a lower-level large-scale trough on the upper-level background QGPV was shown to contribute to the retraction of the jet through negative QGPV advection by the southwesterly winds to the south of the low-level trough minimum. As such, nonlinear interactions at multiple spatial scales acted simultaneously to weaken the jet exit region.

The instantaneous changes in the zonal wind were heavily influenced by mean-flow advection of anomalies, while the cumulative 11–15 February retraction was dominated by nonlinear vortex–vortex interactions – specifically, differential negative  $q'_u$  advection by the winds associated with the  $q'_u$  field itself. The net flux of low QGPV from the Tropics/subtropics northward is commonly the way in which nonlinear advection is viewed as a mechanism that prevents the zonal wind from strengthening in blocking regions (Hoskins *et al.*, 1983; Crum and Stevens, 1988). In this case, negative QGPV anomalies associated with Features A and B were differentially advected *southward* (Figure 7), weakening the zonal wind along the southern edge of the jet core and exit region. Anticyclonic anomalies that reach the poleward side of the jet, as observed in this case and in many other retractions (see fig. 9 from Jaffe *et al.*, 2011), may have a unique ability to influence the zonal wind given the relative position of their associated nonlinear advection fields relative to the jet.

Some advantages to the expanded PTD approach to evaluating geostrophic wind tendencies are that it can be applied to instantaneous, time mean, or spatially filtered data, as

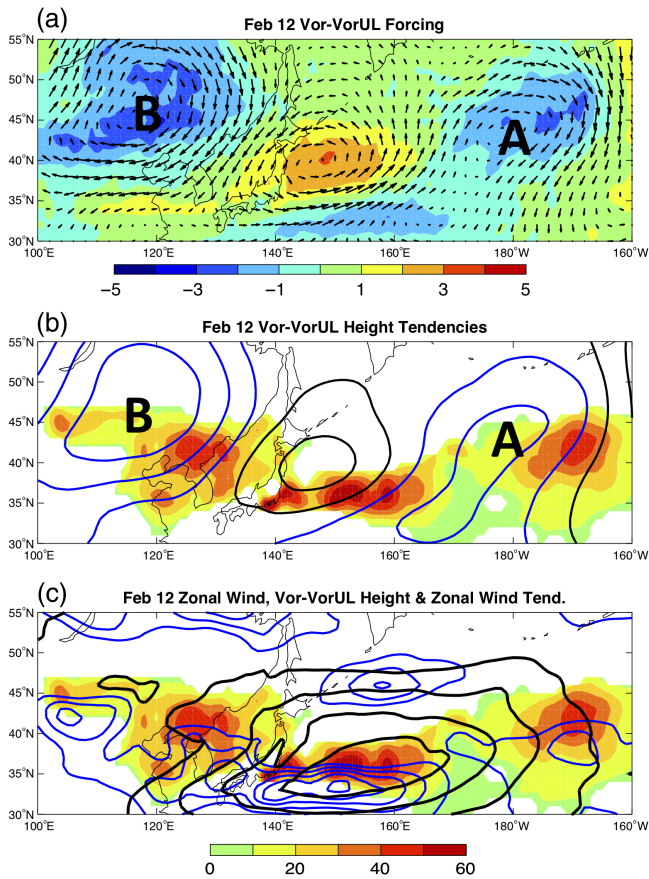


**FIGURE 7** (a) Color shading shows the 12 February average  $q'_u$  field in units of  $10^{-4} \text{ s}^{-1}$ . The black arrows show the 12 February average  $v'_{gu}$  field, which advects  $q'_u$  to produce height tendencies associated with the upper-level nonlinear vortex interaction term. (b) Color shading shows the 12 February averaged height tendencies associated with the forcing implied in (a). Height tendencies are in units  $\text{m} (\text{6 hr})^{-1}$ , with positive values above  $10 \text{ m} (\text{6 hr})^{-1}$  shown. The contours show the 12 February average  $\phi'_u$  field, contoured every  $100 \text{ m}$  with values below zero shown in black, and values of zero and greater in blue. (c) Color shading as in (b), with the blue contours indicating the associated zonal wind tendency, contoured for  $-1, -2, -3, -4$  and  $-5 \text{ m/s} (\text{6 hr})^{-1}$ . The black contours show the 12 February mean zonal wind, contoured every  $10 \text{ m/s}$  beginning at  $30 \text{ m/s}$  [Colour figure can be viewed at [wileyonlinelibrary.com](http://wileyonlinelibrary.com)].

the only assumption made is QGPV conservation. Acceleration of both the zonal and meridional components of the geostrophic wind can be diagnosed in this manner, for stationary or transient features. The expanded PTD method also provides detailed information about the life cycle of eddies *and* their influence on the geostrophic wind, within the same diagnostic framework. Finally, merging QGPV inversion with a zonal wind diagnostic allows for separate quantification of the influence of both lower- and upper-level QGPV structures on the tropopause-level jet. While only the upper-level, nonlinear term contributed to retraction in this case, there is no *a priori* reason that this should be generally true. Admittedly, one limitation to the method is the extent to which QGPV conservation is accurate, a constraint shared by many diagnostics such as those introduced by Hoskins *et al.* (1983), Plumb (1985) and Trenberth (1986).

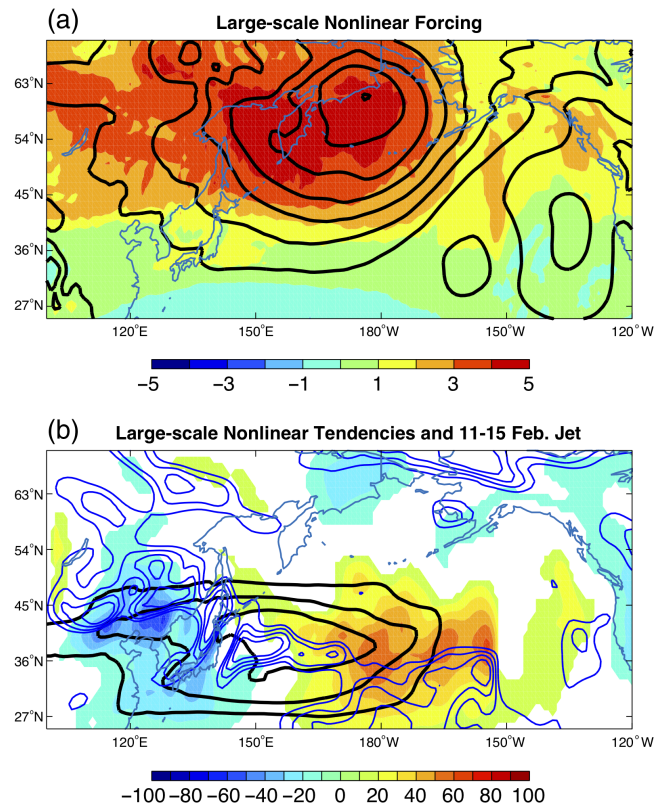


**FIGURE 8** (a) Color shading shows the 11–15 February mean  $300 \text{ hPa } \bar{q}'_u$ , and the black contours show the  $850 \text{ hPa}$  11–15 February average geopotential height field, which is parallel to  $\bar{v}'_g$ . The influence of the low-level circulation, represented by the  $850 \text{ hPa}$  height field, extends to  $300 \text{ hPa}$  and leads to the advection of  $\bar{q}'_u$  by  $\bar{v}'_g$ . Units of  $\bar{q}'_u$  are  $10^{-4} \text{ s}^{-1}$ , and the  $850 \text{ hPa}$  height field is contoured every  $50 \text{ m}$  with lowest heights located east of the Kamchatka peninsula. (b) The colour shading shows the height tendency response to Term  $vi$ ,  $-\bar{v}'_g \cdot \nabla \bar{q}'_u$ , in units of  $\text{m} (\text{6 hr})^{-1}$ . The blue contours represent the corresponding zonal wind tendency, contoured for  $-1, -2, -3$  and  $-4 \text{ m/s} (\text{6 h})^{-1}$ . The  $300 \text{ hPa}$  11–15 February average zonal geostrophic wind is contoured in black, starting at  $30 \text{ m/s}$  every  $10 \text{ m/s}$  [Colour figure can be viewed at [wileyonlinelibrary.com](http://wileyonlinelibrary.com)].

Given that the basic state was defined as a five-day time mean in this study, the contribution to zonal wind tendencies from terms that reference only one anomaly field, i.e. the linear terms, *must* add up to zero when integrating over the five-day period. Given the short time-mean basic state employed, it is possible that linear dynamics are included in our nonlinear terms. However, the same analysis was performed using a wave-number-filtered basic state definition instead (Table 2), and yet the nonlinear terms still dominated the geostrophic zonal wind tendency. Thus, the physical insights resulting from the present analysis, which are consistent with previous studies regarding blocking and nonlinear processes, appear to exhibit only a weak dependence on the basic state definition.

#### 4.1 | Comparison with a traditional zonal wind diagnostic

The importance of nonlinear vortex–vortex interactions in fashioning retraction is consistent with discussion of the

**TABLE 2** Integrated tendency of the zonal wind from 0000 UTC 11 February – 1800 UTC 15 February 2006 using various height tendency fields using a large (<wave number 3) and small scale (>wave number 3) basic state definition

Forcing Term	Zonal Wind Tendency $\text{m s}^{-1}$
<b>SUM PTD:</b>	–35.7843
Term i: Deformation/Superposition	–13.2778
Term ii: Downstream Development	+ 11.9664
Term iii: Baroclinic Development	+ 1.3299
Term iv: Vortex-vortex UL	–23.8889
Term v: Vortex-vortex LL	+ 11.5483
Term vi: large-scale nonlinear interactions	–23.4622

role of nonlinear interactions in changing the low-frequency QGPV as presented by Hoskins *et al.* (1983). They showed that the QG eddy vorticity flux divergence is proportional to the Lagrangian tendency of the low-frequency QGPV in the absence of sources and sinks:

$$(\partial_t + \bar{\mathbf{v}}_{\mathbf{g}} \cdot \nabla) \bar{q} = -\nabla \cdot \overline{\mathbf{v}'_{\mathbf{g}} q'}, \quad (8)$$

In locations where the right-hand side of Equation 8 is negative, the Lagrangian tendency of QGPV is negative. Anywhere the flux convergence is spatially heterogeneous, therefore, changes in the QGPV *gradient*, and by extension the geostrophic wind, must arise. To investigate the relationship between the Eulerian changes in wind speed as diagnosed using Equation 6, versus the Lagrangian change in the QGPV via Equation 8, the 11–15 February average eddy vorticity flux convergence was calculated, using only the  $\mathbf{v}_{\mathbf{gu}}'$  wind field to be consistent with Term *iv*. Next the meridional gradient of that flux convergence, which implies a change in the meridional gradient of the QGPV (and thus to changes in the zonal geostrophic wind), was calculated, with results shown in Figure 9. Negative values of the gradient of the nonlinear eddy vorticity flux lead to a weakening of the low-frequency QGPV gradient moving with the geostrophic flow. Regions where QGPV gradient weakens, and thus where the geostrophic wind would weaken, are observed within the jet core from about 130 to 170°E, 30 to 35°N, and in the entrance region at 100–125°E, 35–40°N (Figure 9). There are indeed regions where the Lagrangian and Eulerian zonal wind tendencies differ; within the vicinity of the jet (130–170°E, 30–45°N), Term *iv* induces a dipole pattern of deceleration and acceleration, while the Lagrangian diagnostic suggests a more detailed tripole pattern (compare Figures 6b and 9).

The change in the jet structure associated with the beginning of retraction is presented in Figure 10, which shows the daily mean QGPV and zonal wind on 11 February (Figure 10a) and 15 February (Figure 10b). It is evident that the QGPV gradient and jet core strengthened to the north and weakened to the south during this period, as the two diagnostics compared in Figures 6 and 9 would suggest. In particular, near-zero PV air was located near 30°N on 11 February, and shifted northward to 40°N by 15 February,

revealing that a northward shift of the jet core accompanied the retraction of the exit region. The jet also became narrower in the meridional direction, changing the environmental shear, which in turn could alter the development of disturbances forming thereafter.

## 4.2 | Conclusions

An important characteristic of the 2006 retraction was related to the propagation of anticyclonic anomalies on the poleward side of the jet and their impact upon the zonal wind. The cumulative influence on the zonal wind of anticyclonic anomalies A and B, and the trough located in between, manifested itself through nonlinear interactions, which dominated the QG zonal wind tendencies from 11 to 15 February. Nonlinear advection was strongest on 12 February, coinciding with the time during which the wave train was most positively tilted (Figure 7b). Mak and Cai (1989) demonstrated that a positively tilted eddy in a region of cyclonic shear, a form of deformation, was conducive to the barotropic growth of the eddy at the expense of the kinetic energy of the environment. Here the retraction, and simultaneous amplification of Feature A (largely due to deformation), indicates that a barotropic energy exchange in which kinetic energy from the environment was transferred to kinetic energy of anomalies, indeed occurred. In fact, the present analysis demonstrates that the winds associated with the upper-level QGPV anomalies are what rearrange the upper-level QGPV anomalies, indicating that the upper-level vortex–vortex term is intrinsically barotropic. Ongoing research suggests that a configuration involving positively tilted height anomalies on the cyclonic shear side of the jet is often observed during jet retractions, for the reasons shown in section 3.1, Figure 7. We find the consistency with previous theoretical research and our observational results of great interest and are not aware of its mention anywhere else in the current literature.

The dominant influence of nonlinear vortex–vortex interactions in facilitating jet retraction, attained through a novel expansion of QG piecewise tendency diagnosis to evaluation of geostrophic wind tendencies, is consistent with the perspective on blocking introduced in Shutts (1983), which emphasized the role of eddy vorticity flux convergence as an important forcing that prevents the westerlies from reforming within the blocking region. More recently, Yamazaki and Itoh (2013) proposed an alternative means by which vortex–vortex interactions can impact the storm track and blocking through a “selective absorption mechanism.” They considered the dominant interaction as one where eddies of different sizes impose different net accelerations on the adjacent eddies. In such a manner they suggested that a blocking anticyclone preferentially “attracts” smaller-scale anticyclones, thus maintaining the block. One key difference between the analysis presented in this study and previous diagnoses of blocking (implied as a negative zonal wind tendency) is the *zonally elongated* band

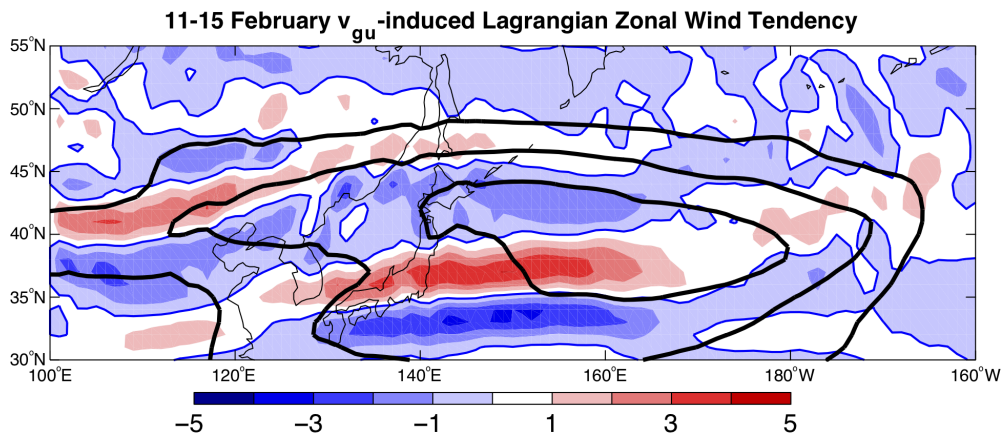


**FIGURE 9** Color shading shows the 11–15 February 2006 mean meridional gradient of the eddy vorticity flux convergence (Equation (8)), calculated using  $v'_{gu}$  to facilitate a direct comparison with Figure 6b. The zero line is contoured in blue. Units are  $10^{-14} \text{ m}^{-1}/\text{s}^2$ . The black contours show the 11–15 February mean geostrophic wind, contoured starting at 30 m/s every 10 m/s [Colour figure can be viewed at [wileyonlinelibrary.com](http://wileyonlinelibrary.com)].

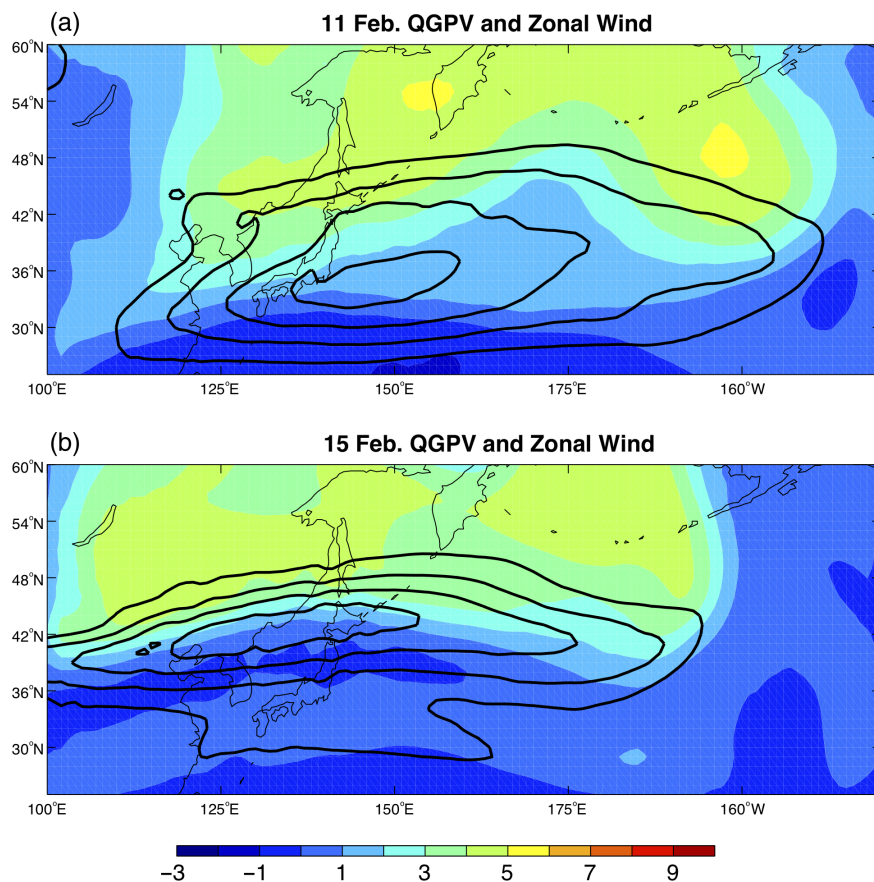


**FIGURE 10** Color shading shows the daily mean QGPV with contours of the zonal geostrophic wind on (a) 11 February and (b) 15 February 2006. Units of QGPV are  $10^{-4} \text{ s}^{-1}$ . Zonal wind contours begin at 30 m/s and increase at intervals of 10 m/s [Colour figure can be viewed at [wileyonlinelibrary.com](http://wileyonlinelibrary.com)].

of height tendencies induced by vortex–vortex interactions, versus the isotropic region of flux convergence more often associated with blocks.

This study has revealed the impact of nonlinear processes on retraction of the North Pacific jet through a novel expansion of the QGPV tendency diagnosis of Nielsen-Gammon and Lefèvre (1996). In this case, vortex–vortex interactions induced by a wave train with the right tilt and position relative to the jet promoted the deceleration of the jet exit region and northward shift of the jet core. Large-scale nonlinear

processes, induced by a low-level trough whose circulation reorganized the upper-level background QGPV, also contributed notably to the deceleration of the jet exit region. There are, it appears, a variety of ways in which nonlinear interactions can alter the circulation. Future work will focus on generalizing these results to retractions in general and expanding the methodology to additional geographic regions. An attempt to forecast such jet stream transitions by viewing the nonlinear PTD terms in real time will also be an avenue of future research.

## ORCID

Melissa Breeden  <https://orcid.org/0000-0001-6298-3696>

## REFERENCES

- Andrews, D.G. and McIntyre, M.E. (1976) Planetary waves in horizontal and vertical shear: the generalized Eliassen–Palm relation and the mean zonal acceleration. *Journal of the Atmospheric Sciences*, 33, 2031–2048. [https://doi.org/10.1175/1520-0469\(1976\)033<2031:PWIHAV>2.0.CO;2](https://doi.org/10.1175/1520-0469(1976)033<2031:PWIHAV>2.0.CO;2).
- Athanasiadis, P.J., Wallace, J.M. and Wettstein, J.J. (2010) Patterns of wintertime jet stream variability and their relation to the storm tracks. *Journal of the Atmospheric Sciences*, 67, 1361–1381. <https://doi.org/10.1175/2009JAS3270.1>.
- Berggren, R., Bolin, B. and Rosaby, C.-G. (1949) An aerological study of zonal motion, its perturbations and break-down. *Tellus*, 1(2), 14–37.
- Berrisford, P., Dee, D.P., Poli, P., Brugge, R., Fielding, K., Fuentes, M., Källberg, P.W., Kobayashi, S., Uppala, S. and Simmons, A. (2011) *The ERA-Interim archive Version 2.0. ERA Report Series 1*. Available at: <http://www.ecmwf.int/en/elibrary/8174-era-interim-archive-version-20> [Accessed September 2016].
- Breeden, M. and Martin, J.E. (2018) Analysis of the initiation of an extreme North Pacific jet retraction using piecewise tendency diagnosis. *Quarterly Journal of the Royal Meteorological Society*, 144(715), 1895–1913. <https://doi.org/10.1002/qj.3388>.
- Crum, F.X. and Stevens, D.F. (1988) A case study of atmospheric blocking using isentropic analysis. *Monthly Weather Review*, 116, 223–241. [https://doi.org/10.1175/1520-0493\(1988\)116<0223:ACSOAB>2.0.CO;2](https://doi.org/10.1175/1520-0493(1988)116<0223:ACSOAB>2.0.CO;2).
- Dee, D.P., Uppala, S.M., Simmons, A.J., Berrisford, P., Poli, P., Kobayashi, S., Andrae, U., Balmaseda, M.A., Balsamo, G., Bauer, P., Bechtold, P., Beljaars, A.C.M., van de Berg, L., Bidlot, J., Bormann, N., Delsol, C., Dragani, R., Fuentes, M., Geer, A.J., Haimberger, L., Healy, S.B., Hersbach, H., Hólm, E.V., Isaksen, I., Källberg, P., Köhler, M., Matricardi, M., McNally, A.P., Monge-Sanz, B.M., Morcrette, J.-J., Park, B.-K., Peubey, C., de Rosnay, P., Tavolato, C., Thépaut, J.-N. and Vitart, F. (2011) The ERA-Interim reanalysis: configuration and performance of the data assimilation system. *Quarterly Journal of the Royal Meteorological Society*, 137(656), 553–597. <https://doi.org/10.1002/qj.828>.
- Eichelberger, S.J. and Hartmann, D.L. (2007) Zonal jet structure and the leading mode of variability. *Journal of Climate*, 20, 5149–5163.
- Ertel, H. (1942) Ein neuer hydrodynamischer Wirbelsatz. *Meteorologische Zeitschrift*, 59, 271–281.
- Evans, K.J. and Black, R.X. (2003) Piecewise tendency diagnosis of weather regime transitions. *Journal of the Atmospheric Sciences*, 60, 1949–1959.
- Frederiksen, J.S. (1983) A unified three-dimensional instability theory of the onset of blocking and cyclogenesis. II. Teleconnection patterns. *Journal of the Atmospheric Sciences*, 40, 2593–2609.
- Griffin, K.S. and Martin, J.E. (2017) Synoptic features associated with temporally coherent modes of variability of the North Pacific jet stream. *Journal of Climate*, 30, 39–54.
- Handlos, Z.J. and Martin, J.E. (2016) Composite analysis of large-scale environments conducive to west Pacific polar/subtropical jet superposition. *Journal of Climate*, 29, 7145–7165.
- Henderson, S.A., Maloney, E.D. and Barnes, E.A. (2016) The influence of the Madden–Julian Oscillation on northern hemisphere winter blocking. *Journal of Climate*, 29, 4597–4616.
- Hoskins, B.J., James, I.N. and White, G.H. (1983) The shape, propagation and mean-flow interaction of large-scale weather systems. *Journal of the Atmospheric Sciences*, 40, 1595–1612.
- Hoskins, B.J. and Sardeshmukh, P.D. (1987) A diagnostic study of the dynamics of the northern hemisphere winter of 1985–86. *Quarterly Journal of the Royal Meteorological Society*, 113, 759–778.
- Jaffe, S.C., Martin, J.E., Vimont, D.J. and Lorenz, D.J. (2011) A synoptic climatology of episodic, subseasonal retractions of the Pacific jet. *Journal of Climate*, 24, 2846–2860.
- Jayawardena, I.M., Chen, Y.L., Nash, A.J. and Kodama, K. (2012) A comparison of three prolonged periods of heavy rainfall over the Hawaiian islands. *Journal of Applied Meteorology*, 51, 722–744.
- Mak, M. and Cai, M. (1989) Local barotropic instability. *Journal of the Atmospheric Sciences*, 46, 3289–3311.
- Martius, O., Schierz, C. and Davies, H.C. (2007) Breaking waves at the tropopause in the wintertime Northern Hemisphere: climatological analyses of the orientation and the theoretical LC1/2 classification. *Journal of the Atmospheric Sciences*, 64, 2576–2592.
- Nakamura, N. and Huang, C.S. (2017) Local wave activity and the onset of blocking along a potential vorticity front. *Journal of the Atmospheric Sciences*, 74, 2341–2362. <https://doi.org/10.1175/JAS-D-17-0029.1>.
- Nielsen-Gammon, J.W. and Lefèvre, R.J. (1996) Piecewise tendency diagnosis of dynamical processes governing the development of an upper-tropospheric mobile trough. *Journal of the Atmospheric Sciences*, 53, 3120–3142.
- Otkin, J.A. and Martin, J.E. (2004) The large-scale modulation of subtropical cyclogenesis in the central and eastern Pacific Ocean. *Monthly Weather Review*, 132, 1813–1828.
- Pfahl, S., Schierz, C., Croci-Maspoli, M., Grams, C.M. and Wernli, H. (2015) Important of latent heat release in ascending air streams for atmospheric blocking. *Nature Geoscience*, 8, 610–614.
- Plumb, R.A. (1985) On the three-dimensional propagation of stationary waves. *Journal of the Atmospheric Sciences*, 42, 217–229. [https://doi.org/10.1175/1520-0469\(1985\)042<0217:OTTDPO>2.0.CO;2](https://doi.org/10.1175/1520-0469(1985)042<0217:OTTDPO>2.0.CO;2).
- Renwick, J.A. and Wallace, J.M. (1996) Relationships between North Pacific Wintertime Blocking, El Niño, and the PNA Pattern. *Monthly Weather Review*, 124, 2071–2076. [https://doi.org/10.1175/1520-0493\(1996\)124<2071:RBNPWB>2.0.CO;2](https://doi.org/10.1175/1520-0493(1996)124<2071:RBNPWB>2.0.CO;2).
- Rex, D.F. (1950) Blocking action in the middle troposphere and its effect upon regional climate. I. An aerological study of blocking action. *Tellus*, 2(3), 196–211.
- Shutts, G.J. (1983) The propagation of eddies in diffluent jetstreams: eddy vorticity forcing of “blocking” flow fields. *Quarterly Journal of the Royal Meteorological Society*, 109, 737–761.
- Trenberth, K.E. (1986) An assessment of the impact of transient eddies on the zonal flow during a blocking episode using localized Eliassen–Palm flux diagnostics. *Journal of the Atmospheric Sciences*, 43, 2070–2087. [https://doi.org/10.1175/1520-0469\(1986\)043<2070:AAOTIO>2.0.CO;2](https://doi.org/10.1175/1520-0469(1986)043<2070:AAOTIO>2.0.CO;2).
- Wallace, J.M. and Gutzler, D.S. (1981) Teleconnections in the geopotential height field during the northern hemisphere winter. *Monthly Weather Review*, 109, 784–812.
- Winters, A.C., Keyser, D. and Bosart, L.F. (2019) The development of the North Pacific Jet Phase Diagram as an objective tool to monitor the state and forecast skill of the upper-tropospheric flow pattern. *Weather and Forecasting*, 34, 199–219. <https://doi.org/10.1175/WAF-D-18-0106.1>.
- Yamazaki, A. and Itoh, H. (2013) Vortex–vortex interactions for the maintenance of blocking. Part I: The selective absorption mechanism and a case study. *Journal of the Atmospheric Sciences*, 70, 725–742.

**How to cite this article:** Breeden M, Martin JE. Evidence for nonlinear processes in fostering a North Pacific jet retraction. *Q J R Meteorol Soc* 2019;145:1559–1570. <https://doi.org/10.1002/qj.3512>